

# Vortex-Induced Injectable Silk Fibroin Hydrogels

Tuna Yucel,<sup>†</sup> Peggy Cebe,<sup>‡</sup> and David L. Kaplan<sup>†\*</sup>

<sup>†</sup>Department of Biomedical Engineering and <sup>‡</sup>Department of Physics and Astronomy, Tufts University, Medford, Massachusetts

**ABSTRACT** A novel, to our knowledge, technique was developed to control the rate of  $\beta$ -sheet formation and resulting hydrogelation kinetics of aqueous, native silk solutions. Circular dichroism spectroscopy indicated that vortexing aqueous solutions of silkworm silk lead to a transition from an overall protein structure that is initially rich in random coil to one that is rich in  $\beta$ -sheet content. Dynamic oscillatory rheology experiments collected under the same assembly conditions as the circular dichroism experiments indicated that the increase in  $\beta$ -sheet content due to intramolecular conformational changes and intermolecular self-assembly of the silk fibroin was directly correlated with the subsequent changes in viscoelastic properties due to hydrogelation. Vortexing low-viscosity silk solutions lead to orders-of-magnitude increase in the complex shear modulus,  $G^*$ , and formation of rigid hydrogels ( $G^* \approx 70$  kPa for 5.2 wt % protein concentration). Vortex-induced,  $\beta$ -sheet-rich silk hydrogels consisted of permanent, physical, intermolecular crosslinks. The hydrogelation kinetics could be controlled easily (from minutes to hours) by changing the vortex time, assembly temperature and/or protein concentration, providing a useful timeframe for cell encapsulation. The stiffness of preformed hydrogels recovered quickly, immediately after injection through a needle, enabling the potential use of these systems for injectable cell delivery scaffolds.

## INTRODUCTION

Many hydrogel materials, both synthetic and natural, have been developed for tissue engineering (1) and drug/growth factor release (2). Synthetic hydrogelating systems can be classified into polymer-based (3), polymer-peptide hybrid (4), and peptidic self-assembling hydrogels (5,6). Peptidic hydrogel systems are promising synthetic materials, since they generally show low immunogenicity and controllable assembly kinetics, nanostructure formation, and hydrogel mechanical properties (7,8). Natural, biopolymeric systems generally show better compatibility for hosting cells and bioactive molecules (4). Among naturally derived biomaterials, silk fibroin hydrogels are of interest for many biomedical applications, such as bone-filling materials (9) and cell encapsulation for three-dimensional cell culture (10).

Generally, several biological (cytocompatibility, cell adhesion, and subsequent morphological changes, cell proliferation, cell phenotype maintenance and in some cases, cell proliferation and postinjection biodegradability of hydrogel matrix) and some physical (bulk mechanical properties as determined by the local and global structure) properties of hydrogel scaffolds are considered to be crucial for cell encapsulation/delivery applications. However, there are additional and challenging materials criteria that should be met before widespread use of these materials for cell delivery applications (7,11). Ideally, hydrogelation kinetics should be controlled precisely to enable homogeneous three-dimensional encapsulation of cells and prevention of cell sedimentation. Once homogeneous cell encapsulation is achieved, an important practical consideration for injectable hydrogel/cell scaffolds is the ease of application into the body with high

spatial precision (7). For example, a shear-thinning hydrogel material could be implanted by minimum invasion to the delivery site, such as by injection through a needle. A hydrogel that shear-thins into a sol during injection could enable more homogeneous delivery of the cells to the wound site as compared to cell delivery in solution. In addition, it would be important for the shear-thinned hydrogel material to recover immediately to a stiff network after removal of applied shear, facilitating localization of a uniform density of cells at the delivery site.

Silk fibroin, the structural, self-assembling protein of silkworm fibers, is a high-molecular-weight block copolymer consisting of a heavy ( $\approx 370$  kDa) and a light ( $\approx 26$  kDa) chain with varying amphiphilicity linked by a single disulfide (12): The heavy chain contains hydrophobic, repetitive oligopeptides rich in alanine and glycine amino acids interspersed with small, more hydrophilic, charged and amorphous regions that give the chain a polyelectrolyte nature. The sequence of the light chain is less repetitive and has a high content of glutamic and aspartic acid residues. Silk fibroin has been processed into a variety of material formats, such as films, electrospun fibers, three-dimensional porous scaffolds, microspheres and hydrogels, mainly for tissue engineering and cell/drug delivery applications (10,13–20). Silk hydrogels have been thoroughly studied for potential biotechnological applications due to their exceptional mechanical properties, biocompatibility, controllable degradation rates, and self-assembly into  $\beta$ -sheet-rich networks (21–25). Previously, self-assembly and concomitant hydrogelation of silk fibroin was triggered in vitro at low pH, high temperatures, or high ionic strength (16,17,19). However, silk gelation was too slow under physiologically relevant solution conditions for the realization of cell encapsulation applications. Recently, an ultrasonication method was introduced that

Submitted May 5, 2009, and accepted for publication July 16, 2009.

\*Correspondence: [david.kaplan@tufts.edu](mailto:david.kaplan@tufts.edu)

Editor: Denis Wirtz.

© 2009 by the Biophysical Society  
0006-3495/09/10/2044/7 \$2.00

doi: 10.1016/j.bpj.2009.07.028

enables rapid and controlled hydrogelation of the silk fibroin in physiological solution conditions for three-dimensional human bone mesenchymal stem-cell encapsulation (10). This method lead to the realization of new tissue engineering applications in the absence of harsh solution conditions that may be detrimental to cell behavior (10).

Silk fibroin is rich in random coil and  $\alpha$ -helical content when produced at high solution concentrations in the silkworm gland. The protein goes through a structural transition into  $\beta$ -sheet-containing fibers during spinning due to elongational and shear forces and the concomitant changes in the ionic concentration and pH (26–30). In addition to leading to changes in protein structure, elongational and shear forces have also been reported to affect the rheological properties of aqueous silk fibroin solutions. For example, an anomalous shear thickening followed by shear-thinning behavior was reported at or above 4.2 wt % silk fibroin concentrations (31), similar to that observed for associating polymers (32,33). This behavior was related to the alignment and stretching of polymer chains induced by the shear-rate gradient and alternating rupture and recovery of the crosslinks. At higher silk concentrations of ~25 wt %, a phase separation between a white, tough material and the surrounding clear liquid was reported at steady shear rates above  $2\text{ s}^{-1}$  (28). This apparent phase separation was attributed to shear-induced crystallization into a  $\beta$ -sheet structure by stretching of fibroin molecules due to the applied flow field and repulsion of bound water at relatively low shear rates as compared to those within the silkworm duct. Interestingly, Kojic and co-workers reported that the mechanical response of the spinning extract of *Nephila clavipes* spider depended strongly on the mode of applied deformation (34): Steady shear experiments showed shear thinning attributable to liquid-crystalline-like alignment of silk protein chains, whereas extensional rheometry showed transient stiffening of the spinning solution, providing important information en route to matching the synthetic silk spinning process to that in nature.

In this article, we present a novel, to our knowledge, and very simple vortexing technique to employ the shear-gradient-induced changes in silk fibroin structure and solution viscoelastic properties to control the postvortex self-assembly and hydrogelation kinetics for cell encapsulation at lower protein concentration than those previously studied. We collected circular dichroism (CD) spectroscopy and dynamic oscillatory rheology data under the same assembly conditions at the same time points after triggering hydrogelation by vortexing. Hence, isotemporal evolution of the shear-induced changes in the overall protein structure due to changes in molecular conformation and intermolecular self-assembly could be correlated to concomitant changes in viscoelastic properties due to vortex-induced hydrogelation. In addition, we study the shear-thinning and recovery behavior of vortex-induced silk hydrogels using rheology to highlight the suitability of these materials as versatile cell delivery scaffolds.

## MATERIALS AND METHODS

### Preparation of aqueous silk fibroin solutions

Silk fibroin aqueous solutions were prepared as previously described (35). Briefly, *Bombyx mori* cocoons were boiled for 40 min in an aqueous solution of 0.02 M sodium carbonate and then rinsed thoroughly with deionized water. After overnight drying, the silk fibroin was dissolved in an aqueous solution containing 9.3 M LiBr at 60°C overnight. The solution was dialyzed against deionized water using Slide-a Lyzer dialysis cassettes (MWCO 3500, Pierce, Rockford, IL) for two days to remove the residual salt. The final concentration of the silk fibroin was ~5.2 wt %. Lower concentration silk solutions were prepared by diluting the 5.2 wt % stock solution with deionized water.

### Vortex-induced hydrogelation

In a typical CD spectroscopy or rheology experiment, 1 mL of silk solution was equilibrated at 25°C in a vial kept in a water bath for 10 min and mixed for predetermined times at 3200 rpm using a vortexer (Fisher Scientific, Hampton, NH) to induce silk self-assembly and hydrogelation. Increasing the vortex time increased the solution turbidity and eventually bulk phase separation of a white and solidlike material was observed, especially at lower protein concentrations. Both CD and rheology data were collected from turbid solutions after removal of the solid phase.

### Circular dichroism (CD) spectroscopy

Circular dichroism (CD) spectra were collected using an AVIV Biomedical Model 410 CD spectrometer (Lakewood, NJ). After vortexing, aqueous silk solutions were immediately loaded in a 0.1 mm quartz cell within a temperature-controlled cell holder. CD wavelength scans between 210 and 260 nm or time sweeps at 216 nm were collected at 25°C. Due to the high silk concentrations, the high dynode voltages below 210 nm lead to erroneous data. The CD spectrum of water collected immediately before each measurement was used for background correction. The mean residual ellipticity was calculated from

$$[\theta] = \frac{\theta \cdot M}{10 \cdot c \cdot l \cdot n} \left( \frac{\text{deg} \cdot \text{cm}^2}{\text{dmol}} \right),$$

where  $\theta$  is the measured ellipticity (deg),  $M$  is the mean molecular mass (g/mol),  $c$  is the protein concentration (g/cm<sup>3</sup>),  $l$  is the path length (cm), and  $n$  is the number of residues.  $M$  and  $n$  for *B. mori* heavy chain were taken as 391,563 g/mol and 5263, respectively (36) (Accession: P05790). For protein concentration measurements, a 0.5 mL aliquot of silk solution was dried at 60°C overnight and the solution concentration was calculated from the weight of the dried film.

### Dynamic oscillatory rheology

Dynamic oscillatory time, frequency and strain sweeps were performed using an ARES strain-controlled rheometer (TA Instruments, New Castle, DE) with 25- or 50-mm-diameter stainless steel parallel plate geometries at 0.5-mm measuring gap distance. In a typical experiment, the silk solution was applied slowly via a syringe on the rheometer plate to prevent shearing of the sample immediately after vortexing. The normal force applied on the sample during lowering of the top plate was limited to 0.1 N. A low viscosity mineral oil and the solvent trap supplied by TA instruments were used to prevent sample evaporation from the sides of the plate. Dynamic oscillatory time sweeps were collected at a low strain amplitude ( $\gamma = 1\%$ ,  $\omega = 10\text{ rad/s}$ ) to prevent possible sample manipulation due to applied shear during measurements. Frequency sweeps were collected over a wide frequency range ( $\gamma = 1\%$ ,  $\omega = 0.1\text{--}100\text{ rad/s}$ ) after each time sweep. To observe the time evolution of the frequency dependence of viscoelastic properties, frequency sweeps were collected continuously over a narrower range

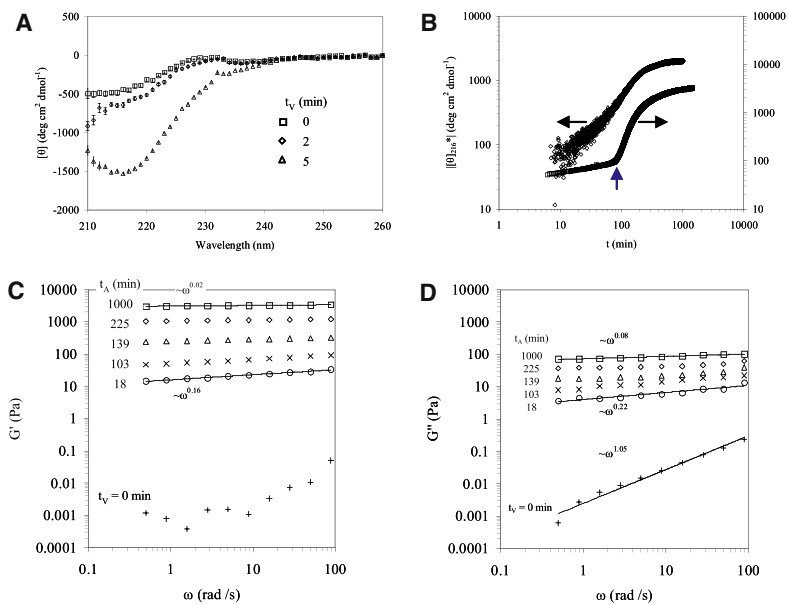


**FIGURE 1** (A) Far-UV CD spectra collected immediately after vortexing silk solutions for different durations,  $t_V$ . (B) Correlation between the time evolution of the increase in  $[\theta]_{216}$  measured by CD and the shear storage modulus,  $G'$  measured by dynamic oscillatory rheology during postvortex incubation. Rheology frequency sweeps of (C) storage and (D) loss modulus collected at different postvortex assembly times,  $t_A$ , under the same assembly conditions as in panel B. The frequency sweep data collected from nonvortexed silk solution was also given in panels C and D for comparison (+).

( $\gamma = 1\%$ ,  $\omega = 0.5\text{--}100 \text{ rad/s}$ ). At the applied shear amplitude, continuous collection of frequency sweeps had no detectable effect on the measured rheological properties. Strain sweep measurements were performed from  $\gamma = 0.01\text{--}1000\%$  ( $\omega = 10 \text{ rad/s}$ ) at the end of each experiment to determine the linear viscoelastic regime of the final hydrogel.

## Injection studies

To study the injectability of vortexed hydrogels and the shear-recovery behavior, vortexed silk solutions were either loaded into 1 mL syringes immediately after vortexing and allowed to gel overnight, or were loaded into syringes after overnight hydrogelation in vials. A 21-gauge needle was connected to the syringe, and the hydrogel was injected through the needle directly onto the rheometer plate. A frequency sweep was collected over a wide frequency range ( $\gamma = 1\%$ ,  $\omega = 0.1\text{--}100 \text{ rad/s}$ ) within 10 min of injection of the sample.

## RESULTS AND DISCUSSION

### Vortexing triggers $\beta$ -sheet formation

Fig. 1 A shows far-UV CD spectra collected from aqueous native silk solutions with a protein concentration,  $\varphi = 1.3 \text{ wt } \%$  at  $25^\circ\text{C}$ , immediately after vortexing for different times,  $t_V$ . Nonvortexed silk solution did not show any local minima attributable to  $\alpha$ -helical or  $\beta$ -sheet conformations within the observed wavelength range ( $210 \text{ nm} < \lambda < 260 \text{ nm}$ ), indicating that the molecular conformation is predominantly random-coil in solution. Vortexing the silk solution for 2 min ( $t_V = 2 \text{ min}$ ) lead to a detectable increase in the apparent  $\beta$ -sheet content, as observed by the formation of a local minimum at  $\lambda = 216 \text{ nm}$  in the measured mean residual ellipticity values ( $[\theta]_{216}$ ). With increasing vortex time ( $t_V = 5 \text{ min}$ ), the absolute value of  $[\theta]_{216}$  increased further, suggesting an increase in the overall  $\beta$ -sheet content. The increase in  $\beta$ -sheet content measured by CD was associated with an increase in solution turbidity. The increase in turbidity was presumably due to increasing concentration

fluctuations caused by the increased shear-gradient due to vortexing (see Possible Hydrogelation Mechanism, below) leading to the dispersion of micron-scale,  $\beta$ -sheet rich silk macromolecule clusters in solution. At lower protein concentrations, longer vortexing times lead to the formation of bulk phase-separated agglomerates.

### Overall molecular conformation and viscoelastic properties

Fig. 1 B shows the dependence of  $\beta$ -sheet content detected by CD spectroscopy and the shear storage modulus,  $G'$ , measured by dynamic oscillatory rheology on postvortex assembly time,  $t_A$  ( $25^\circ\text{C}$ ,  $\varphi = 2.6 \text{ wt } \%$  and  $t_V = 7 \text{ min}$ ). Here,  $[\theta]_{216}^*$  was calculated by subtracting the  $[\theta]_{216}$  value obtained from nonvortexed silk solution rich in random coil content from the  $[\theta]_{216}$  value measured from the sample to observe the evolution of  $\beta$ -sheet content due to silk self-assembly. The time progress of  $[\theta]_{216}^*$  and  $G'$  were very similar, showing a gradual increase with increasing assembly time. In a double logarithmic scale,  $G'$  initially increased gradually, followed by a rapid increase in  $G'$  after  $t_A \approx 100 \text{ min}$ . This orders-of-magnitude increase in  $G'$  may indicate a percolationlike transition due to increasing connectivity of  $\beta$ -sheet rich macromolecule clusters to form a hydrogel network. Overall, a strong correlation was apparent between the increasing  $\beta$ -sheet content due to changes in molecular conformation and intermolecular self-assembly, possibly leading to macromolecular cluster formation and the subsequent increase in the elasticlike behavior, presumably due to increasing intercluster interactions.

Fig. 1, C and D, show the time evolution of the dynamic frequency sweeps of the shear storage ( $G'$ ) and loss modulus ( $G''$ ) during postvortex self-assembly collected under the same assembly conditions as in Fig. 1 B. Nonvortexed silk

fibroin solution essentially behaved as a low viscosity, Newtonian fluid within the measured frequencies (dynamic complex viscosity,  $\eta^* \approx 3 \text{ mPa s}$ ). There was a significant increase in the elasticlike behavior immediately after vortexing: Both  $G'$  and  $G''$  increased by orders of magnitude, with  $G' > G''$  at all measured frequencies.  $G'$  showed a weaker frequency dependence than  $G''$  ( $G' \propto \omega^{0.16}$  and  $G'' \propto \omega^{0.22}$ ), suggesting that the macromolecule clusters could essentially behave as viscoelastic fluids displaying gel-like behavior within the observed frequency range. The apparent gel-like behavior may be attributed to the relatively large size of the micron-scale macromolecule clusters. With increasing assembly time after vortexing, there was a gradual increase in both  $G'$  and  $G''$  which showed progressively weaker frequency dependence, especially after the apparent percolation transition of the clusters at  $t \approx 100 \text{ min}$ .  $G'$  and  $G''$  became essentially frequency-independent within the measured frequency range after  $t_A^* \approx 1000 \text{ min}$  of assembly ( $G' \propto \omega^{0.02}$  and  $G'' \propto \omega^{0.08}$ ), suggesting the formation of a hydrogel network consisting of permanent intercluster physical crosslinks (8).

### Possible hydrogelation mechanism

Shear-induced gelation has been reported for polymers in poor solvents (37) and amphiphilic, associating polymers (32,33). For polymers in poor solvents, shear flow is believed to increase the concentration fluctuations, which may lead to the assembly of macromolecules in the absence of excluded volume in a poor solvent (37). For associating polymers, increased intermolecular interactions between self-associating chains that undergo non-Gaussian stretching due to flow were argued to lead to shear-induced gelation (33). The silk protein is an amphiphilic, block copolymer that consists of segments with predominantly hydrophobic domains that are phase-separated in the nanometer scale to enable solubilization in water (38). Based on overall hydrophobicity of silk fibroin (in the absence of the nanophase-separated, folded molecular arrangement), water could be considered as a poor solvent for this protein. For example, viscoelastic characterization of silk fibroin solutions in  $\text{LiBr}\cdot\text{H}_2\text{O}/\text{H}_2\text{O}/\text{C}_2\text{H}_5\text{OH}$  mixed solvents showed that the solution dynamic viscosity and flow activation energy decrease, while dissolution time and the concentration of LiBr necessary to dissolve silk fibroin increase with increasing water content, suggesting that water acts as the poor solvent in this solvent system (39,40). Therefore, a shear-induced hydrogelation mechanism analogous to that proposed for polymers in poor solvents and amphiphilic-associating polymers could be operational in the vortex-induced hydrogelation of the silk fibroin. Namely, vortexing could increase the concentration fluctuations in the aqueous silk solution, which could lead to self-assembly into clusters and increased intercluster interactions in the absence of excluded volume. It can be argued that the spatial heteroge-

neity of concentration fluctuations or a shear gradient may be responsible for controlling the kinetics of native silk hydrogelation: The shear-gradient may cause non-Gaussian stretching (unfolding) of silk fibroin molecular domains and formation of macromolecule clusters rich in  $\beta$ -sheet content due to increased exposure of hydrophobic domains to water. Increasing size and concentration of  $\beta$ -sheet macromolecule clusters, and subsequent increase in the concentration and overall lifetime of intercluster crosslinks and the physical entanglements between dangling fibroin chains, could eventually lead a percolationlike transition into a permanent, physical hydrogel network.

### Controlling hydrogelation kinetics and final hydrogel rigidity

Hydrogelation kinetics could be controlled easily by changing the processing parameters, such as vortex time (Fig. 2, A and B), postvortex assembly temperature (Fig. 2, C and D), and silk concentration (Fig. 2, E and F). This way, self-assembly and hydrogelation kinetics were adjusted from minutes to hours to potentially enable homogeneous encapsulation of cells in three dimensions; namely, cells could be introduced immediately before the rapid gelation due to the apparent percolation transition to prevent cell sedimentation. It should be noted here that the shear storage modulus ( $G'$ ) values at the apparent percolation were in a rather narrow range between 30 and 100 Pa (at 10 rad/s) for most studied assembly conditions, giving a rough estimate of the solution viscoelastic properties when the cells could be introduced for homogeneous encapsulation. Fig. 2, A and B, show the time evolution of  $G'$  and the shear loss modulus ( $G''$ ), respectively, after vortexing the solutions for different times,  $t_V$  ( $25^\circ\text{C}$ ,  $\varphi = 5.2 \text{ wt \%}$ ). There was a noted increase in the initial  $G'$  values immediately after vortexing with increasing vortex time, presumably due to increasing concentration of macromolecule clusters. Moreover, the apparent jump in  $G'$  attributed to increasing cluster connectivity shifted to shorter assembly times, i.e.,  $t_A^*$  decreased with increasing vortex time ( $t_A^* \approx 35, \approx 50, \approx 100, \text{ and } > 1000 \text{ min}$  for  $t_V = 11, 9, 7, \text{ and } 0 \text{ min}$ , respectively). However, the increase in stiffness after  $t_A^*$  was slower with increasing vortex time and the apparent equilibrium stiffness of the final hydrogel was essentially independent of the vortex time. Therefore, vortexing provided a useful means for controlling the assembly kinetics of the native silk and did not significantly alter the final mechanical properties of the self-assembled silk hydrogels.

Fig. 2, C and D, show the time evolution of rheological properties at different assembly temperatures ( $\varphi = 5.2 \text{ wt \%}$ ,  $t_V = 7 \text{ min}$ ). The self-assembly and hydrogelation kinetics of vortexed silk solutions could easily be increased by increasing the assembly temperature. A master curve of the  $G'$  data shown in Fig. 2 C could be constructed by normalizing the assembly time by a time shift factor,  $t_0$ , indicating

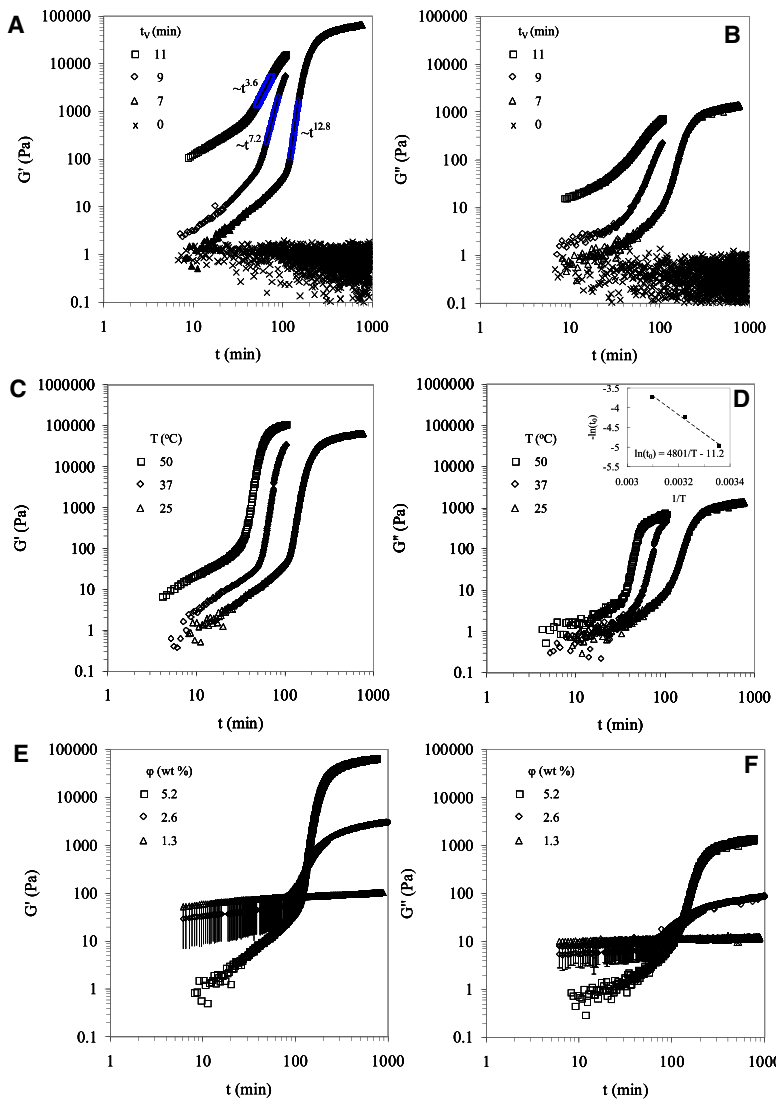


**FIGURE 2** Controlling hydrogelation kinetics by vortex time (A and B), assembly temperature (C and D), and protein concentration (E and F) (see text for experimental details and assembly conditions). Power law exponents in panel A were obtained from fits to  $G'$  data immediately after the apparent percolation.

that the self-assembly mechanism at different temperatures may be similar within the studied temperature range (data not shown). As a further note, an Arrhenius type plot showed a linear dependence of the time-shift factor as a function of reciprocal assembly temperature

$$\ln(t_0) = \frac{4801}{T} - 11.2$$

(Fig. 2 D, inset). For comparison, the time evolution of  $G'$  and  $G''$  for the nonvortexed solution at 50°C were also given in Fig. 2 A, which showed no detectable change in the viscoelastic behavior after 1000 min, indicating the significant effect of vortexing on hydrogelation kinetics.

Fig. 2, E and F, show the time evolution of the viscoelastic properties for different silk concentrations (25°C for  $t_V = 7$  min). The final hydrogel stiffness was strongly dependent on the initial protein concentration: For low protein concentrations ( $0.32 < \varphi < 1.3$  wt %)  $G' \propto \varphi^{1.5}$ , while at higher protein concentrations ( $1 < \varphi < 5.2$  wt %)  $G' \propto \varphi^4$  (data

not shown). The concentration dependence of network stiffness of vortexed silk hydrogels in the high-concentration regime resembles that in shear-induced gelation of amphiphilic polymers in the entangled regime ( $G' \propto \varphi^{3.7}$ ) (32). A much weaker theoretical concentration dependence ( $G' \propto \varphi^{2.5}$ ) was observed for highly crosslinked, semiflexible biopolymer chain networks (41). The initial  $G'$  values after vortexing apparently increased with decreasing silk concentration. This observation could be attributed to the increasing effect of vortex-induced concentration fluctuations and formation of a higher concentration of macromolecule clusters with decreasing protein concentration.

### Hydrogel stiffness recovers after shear-thinning

Another important practical consideration for injectable hydrogel/cell scaffolds could be the ease of application to the body with high spatial precision, e.g., by injection through a needle. We first examined possible shear-thinning behavior

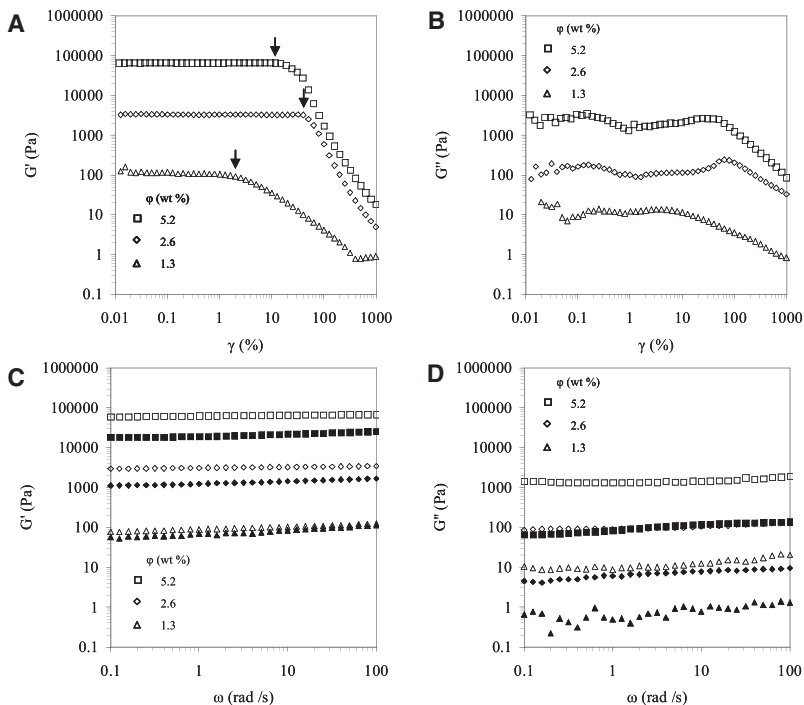


FIGURE 3 Strain sweeps (A and B) collected from vortex-induced hydrogels with different silk concentrations (arrows show apparent yielding). Frequency (C and D) sweeps collected from the hydrogels before (open symbols) and immediately after shear-thinning by injection through a 21-gauge needle (solid symbols).

in vortex-induced hydrogels formed on the rheometer plate. Fig. 3, A and B, show the dependence of  $G'$  and  $G''$  on the amplitude of the applied shear as a function of protein concentration. All hydrogels display a linear viscoelastic regime and apparently yield above the shear amplitude,  $\gamma_B$  ( $\gamma_B \approx 2\%$ ,  $\approx 40\%$ , and  $\approx 10\%$  for 1.3 wt %, 2.6 wt %, and 5.2 wt % hydrogels, respectively) followed by apparent shear-thinning. Shear-thinning could be attributed to the rupture of dangling chain entanglement crosslinks and breaking apart of clusters from the hydrogel network at high shear amplitude. From a practical viewpoint, shear-thinning of the hydrogel (e.g., during injection *in vivo*) could enable a more homogeneous delivery of the cells in the shear-thinned sol to the wound site as compared to cell delivery in solution (7). The apparent decrease in  $\gamma_B$  from 2.6 wt % to 5.2 wt % could be due to formation of a slip layer at the hydrogel/rheometer plate interface at high shear for very stiff hydrogels leading to an underestimation of  $\gamma_B$ .

To study possible recovery of crosslinks in vortexed hydrogels after shear-thinning, we compared frequency sweeps collected before and immediately after directly injecting the gels through a 21-gauge needle onto the rheometer plate (Fig. 3, C and D). Injection through a needle was chosen to demonstrate the possibility of injection of the hydrogels in a minimally invasive manner to a delivery site. For all hydrogels, there was significant recovery of stiffness immediately after injection (for  $\varphi = 1.3$  wt %,  $G'$  recovered almost to the preinjection value, while for higher protein concentrations,  $G' \approx 1/3$  of the preinjection value). All hydrogels essentially displayed frequency-independent shear modulus immediately after cessation of applied shear due to injection. It is unlikely that the shear-recovery of vortexed hydrogels

after shear-thinning is due to the disruption and reformation of permanent, intermolecular  $\beta$ -sheet crosslinks. Therefore, the presence of another crosslinking mechanism in addition to the intermolecular  $\beta$ -sheet crosslinks could be hypothesized similar to that proposed for  $\beta$ -hairpin peptide hydrogels (7,8,11): For example, large,  $\beta$ -sheet rich clusters could slide past each other during shear-thinning by the temporary release of permanent, intercluster, dangling chain entanglements at high shear amplitudes, which may re-form after removal of shear, with no significant change in the overall  $\beta$ -sheet content. Overall, considering the high stiffness values and the frequency independence of viscoelastic properties immediately after injection, we would expect these materials to facilitate localization of cells at the injection site with high spatial precision.

## CONCLUSIONS

In this article, we presented a novel, to our knowledge, method to control the rate of  $\beta$ -sheet formation and resulting hydrogelation kinetics of aqueous silk solutions to within a timeframe that should enable homogeneous cell encapsulation in three dimensions. The novel vortexing technique is simple, yet versatile. Hydrogelation kinetics could be controlled easily by changing the vortex time, assembly temperature, and/or protein concentration. Vortex-induced hydrogels shear-thinned during injection through needles, while hydrogel stiffness recovered immediately after the removal of applied shear. Physicochemical characterization presented in this article will be further correlated with cell behavior to study the applicability of these materials for homogeneous three-dimensional cell encapsulation, homogeneous

delivery in vivo, and localization of hydrogel/cell scaffolds at the injection site.

We thank the National Institutes of Health via the Tissue Engineering Resource Center (grant No. P41 EB002520) and The Air Force Office of Scientific Research for support.

## REFERENCES

- Lee, K. Y., and D. J. Mooney. 2001. Hydrogels for tissue engineering. *Chem. Rev.* 101:1869–1879.
- Langer, R. 2000. Biomaterials in drug delivery and tissue engineering: one laboratory's experience. *Acc. Chem. Res.* 33:94–101.
- Anseth, K. S., A. T. Metters, S. J. Bryant, P. J. Martens, J. H. Elisseeff, et al. 2001. In situ forming degradable networks and their application in tissue engineering and drug delivery. In 10th International Symposium on Recent Advances in Drug Delivery Systems. Elsevier Science Bv, Salt Lake City, Utah.
- Lutolf, M. P., and J. A. Hubbell. 2005. Synthetic biomaterials as instructive extracellular microenvironments for morphogenesis in tissue engineering. *Nat. Biotechnol.* 23:47–55.
- Pochan, D. J., J. P. Schneider, J. Kretsinger, B. Ozbas, K. Rajagopal, et al. 2003. Thermally reversible hydrogels via intramolecular folding and consequent self-assembly of a de novo designed peptide. *J. Am. Chem. Soc.* 125:11802–11803.
- Schneider, J. P., D. J. Pochan, B. Ozbas, K. Rajagopal, L. Pakstis, et al. 2002. Responsive hydrogels from the intramolecular folding and self-assembly of a designed peptide. *J. Am. Chem. Soc.* 124:15030–15037.
- Haines-Butterick, L., K. Rajagopal, M. Branco, D. Salick, R. Rughani, et al. 2007. Controlling hydrogelation kinetics by peptide design for three-dimensional encapsulation and injectable delivery of cells. *Proc. Natl. Acad. Sci. USA*. 104:7791–7796.
- Yucel, T., C. M. Micklitsch, J. P. Schneider, and D. J. Pochan. 2008. Direct observation of early-time hydrogelation in  $\beta$ -hairpin peptide self-assembly. *Macromolecules*. 41:5763–5772.
- Fini, M., A. Motta, P. Torricelli, G. Glavaresi, N. N. Aldini, et al. 2005. The healing of confined critical size cancellous defects in the presence of silk fibroin hydrogel. *Biomaterials*. 26:3527–3536.
- Wang, X. Q., J. A. Kluge, G. G. Leisk, and D. L. Kaplan. 2008. Sonication-induced gelation of silk fibroin for cell encapsulation. *Biomaterials*. 29:1054–1064.
- Yucel, T. 2008. Early-time,  $\beta$ -hairpin self-assembly and hydrogelation: structure, kinetics and shear-recovery. PhD Dissertation in Materials Science and Engineering. University of Delaware, Newark.
- Inoue, S., K. Tanaka, F. Arisaka, S. Kimura, K. Ohtomo, et al. 2000. Silk fibroin of *Bombyx mori* is secreted, assembling a high molecular mass elementary unit consisting of H-chain, L-chain, and P25, with a 6:6:1 molar ratio. *J. Biol. Chem.* 275:40517–40528.
- Hino, T., M. Tanimoto, and S. Shimabayashi. 2003. Change in secondary structure of silk fibroin during preparation of its microspheres by spray-drying and exposure to humid atmosphere. *J. Colloid Interface Sci.* 266:68–73.
- Jin, H. J., S. V. Fridrikh, G. C. Rutledge, and D. L. Kaplan. 2002. Electrospinning *Bombyx mori* silk with poly(ethylene oxide). *Biomacromolecules*. 3:1233–1239.
- Jin, H. J., J. Park, R. Valluzzi, P. Cebe, and D. L. Kaplan. 2004. Biomaterial films of *Bombyx mori* silk fibroin with poly(ethylene oxide). *Biomacromolecules*. 5:711–717.
- Kim, U. J., J. Y. Park, C. M. Li, H. J. Jin, R. Valluzzi, et al. 2004. Structure and properties of silk hydrogels. *Biomacromolecules*. 5:786–792.
- Matsumoto, A., J. Chen, A. L. Collette, U. J. Kim, G. H. Altman, et al. 2006. Mechanisms of silk fibroin sol-gel transitions. *J. Phys. Chem. B*. 110:21630–21638.
- Nazarov, R., H. J. Jin, and D. L. Kaplan. 2004. Porous 3-D scaffolds from regenerated silk fibroin. *Biomacromolecules*. 5:718–726.
- Wang, H., Y. P. Zhang, H. L. Shao, and X. C. Hu. 2005. A study on the flow stability of regenerated silk fibroin aqueous solution. *Int. J. Biol. Macromol.* 36:66–70.
- Wang, X. Q., E. Wenk, A. Matsumoto, L. Meinel, C. M. Li, et al. 2007. Silk microspheres for encapsulation and controlled release. *J. Control. Release*. 117:360–370.
- Altman, G. H., F. Diaz, C. Jakuba, T. Calabro, R. L. Horan, et al. 2003. Silk-based biomaterials. *Biomaterials*. 24:401–416.
- Horan, R. L., K. Antle, A. L. Collette, Y. Z. Huang, J. Huang, et al. 2005. In vitro degradation of silk fibroin. *Biomaterials*. 26:3385–3393.
- Ishida, M., T. Asakura, M. Yokoi, and H. Saito. 1990. Solvent-induced and mechanical-treatment-induced conformational transition of silk fibroins studied by high-resolution solid-state C-13 NMR spectroscopy. *Macromolecules*. 23:88–94.
- Jin, H. J., and D. L. Kaplan. 2003. Mechanism of silk processing in insects and spiders. *Nature*. 424:1057–1061.
- Kim, U. J., J. Park, H. J. Kim, M. Wada, and D. L. Kaplan. 2005. Three-dimensional aqueous-derived biomaterial scaffolds from silk fibroin. *Biomaterials*. 26:2775–2785.
- Chen, X., D. P. Knight, and F. Vollrath. 2002. Rheological characterization of *Nephila spidroin* solution. *Biomacromolecules*. 3:644–648.
- Dicko, C., F. Vollrath, and J. M. Kenney. 2004. Spider silk protein refolding is controlled by changing pH. *Biomacromolecules*. 5:704–710.
- Terry, A. E., D. P. Knight, D. Porter, and F. Vollrath. 2004. PH induced changes in the rheology of silk fibroin solution from the middle division of *Bombyx mori* silkworm. *Biomacromolecules*. 5:768–772.
- Vollrath, F., and D. P. Knight. 2001. Liquid crystalline spinning of spider silk. *Nature*. 410:541–548.
- Zhou, L., X. Chen, Z. Z. Shao, Y. F. Huang, and D. P. Knight. 2005. Effect of metallic ions on silk formation the mulberry silkworm, *Bombyx mori*. *J. Phys. Chem. B*. 109:16937–16945.
- Ochi, A., K. S. Hossain, J. Magoshi, and N. Nemoto. 2002. Rheology and dynamic light scattering of silk fibroin solution extracted from the middle division of *Bombyx mori* silkworm. *Biomacromolecules*. 3:1187–1196.
- Cadix, A., C. Chassenieux, F. Lafuma, and F. Lequeux. 2005. Control of the reversible shear-induced gelation of amphiphilic polymers through their chemical structure. *Macromolecules*. 38:527–536.
- Witten, T. A., and M. H. Cohen. 1985. Cross-linking in shear-thickening ionomers. *Macromolecules*. 18:1915–1918.
- Kojic, N., J. Bico, C. Clasen, and G. H. McKinley. 2006. Ex vivo rheology of spider silk. *J. Exp. Biol.* 209:4355–4362.
- Sofia, S., M. B. McCarthy, G. Gronowicz, and D. L. Kaplan. 2001. Functionalized silk-based biomaterials for bone formation. *J. Biomed. Mater. Res.* 54:139–148.
- Zhou, C. Z., F. Confalonieri, N. Medina, Y. Zivanovic, C. Esnault, et al. 2000. Fine organization of *Bombyx mori* fibroin heavy chain gene. *Nucleic Acids Res.* 28:2413–2419.
- Onuki, A. 1997. Phase transitions of fluids in shear flow. *J. Phys. Condens. Matter*. 9:6119–6157.
- Bini, E., D. P. Knight, and D. L. Kaplan. 2004. Mapping domain structures in silks from insects and spiders related to protein assembly. *J. Mol. Biol.* 335:27–40.
- Matsumoto, K., and H. Uejima. 1997. Regenerated protein fibers. 1. Research and development of a novel solvent for silk fibroin. *J. Polym. Sci. Pol. Chem.* 35:1949–1954.
- Matsumoto, K., H. Uejima, Y. Sano, and H. Sumino. 1997. Regenerated protein fibers. 2. Viscoelastic behavior of silk fibroin solutions. *J. Polym. Sci. Pol. Chem.* 35:1955–1959.
- Mackintosh, F. C., J. Kas, and P. A. Janmey. 1995. Elasticity of semi-flexible biopolymer networks. *Phys. Rev. Lett.* 75:4425–4428.